International Journal of Thermophysics, Vol. 27, No. 5, September 2006 (© 2006)
DOI: 10.1007/s10765-006-0125-3

Thermophysical Properties of Nitrogen from a New Potential Energy Surface Using the Mason–Monchick Approximation

M. H. Karimi Jafari[1] and A. Maghari[1,2]

Received January 04, 2006

A recent N_2–N_2 potential has been used to calculate the second virial, viscosity, and diffusion coefficients. Calculations have been done up to the first quantum correction for virial coefficients and the second-order kinetic theory approximation for transport coefficients. The Mason–Monchick approximation (MMA) has been used for the calculation of collision integrals and, via a numerical analysis, a common intersection point has been found for reduced cross sections and collision integrals of different orientations. This regularity has been interpreted with the aim of the orientation dependence of the potential energy and different types of collisions between molecules. The overall agreement of the calculated second virial coefficient with experiment is reasonable but suggests that a slight re-scaling of the potential would be beneficial. In the case of transport properties, calculated and experimental results show an average deviation of about 1.6% and 0.7% for viscosity and relative diffusion coefficients, respectively.

KEY WORDS: collision integrals; diffusion; Mason–Monchick approximation; second virial coefficient; viscosity.

1. INTRODUCTION

The interaction energy of molecules is an important basic property that is essential for many studies. Nowadays the calculation of intermolecular forces is facilitated by routine quantum chemical methods. In this direction, we have recently obtained a detailed anisotropic N_2–N_2 potential

[1] Department of Physical Chemistry, University College of Science, University of Tehran, Tehran, Iran.
[2] To whom correspondence should be addressed. E-mail: maghari@khayam.ut.ac.ir

energy surface (PES) from *ab initio* calculations at the MP2/QZ level of theory, and this surface has been represented analytically [1]. It has been predicted that this PES might be relatively near the exact one, since the oscillatory behavior of the MP series up to second order results in an underestimation of the interaction energy, which can be compensated by the incompleteness error of the basis set employed. For our proposed potential, however, it is crucial to test its ability to reproduce experimental properties. Among various macroscopic properties, second virial and transport coefficients usually are appropriate candidates. The Wigner–Kirkwood expansion in $\hbar^2$ is suitable for the computation of the second virial coefficient. In particular, Pack [2] developed a formalism for the first-order quantum correction in $\hbar^2$. To calculate the viscosity and diffusion coefficients, we have used the procedure known as the Mason–Monchick approximation (MMA) [3], which is the classical counterpart of the infinite-order-sudden (IOS) approximation of quantal inelastic scattering [4]. Essentially equivalent calculations, with different surfaces, have been performed by Stallcop et al. [5]. Thus, we also present a detailed analysis of MMA to answer some questions about it.

In Section 2, we explain some methodological aspects of this work and corresponding formulas. Comparisons of calculated second virial, viscosity, and diffusion coefficients with experimental data are presented in Section 3. This section also contains a detailed numerical analysis of the MMA procedure.

2. METHOD

2.1. Ab Initio N_2–N_2 Potential

Details of the *ab initio* calculations leading to the N_2–N_2 potential have been described in our previous work [1]. A step-by-step fitting strategy has been designed to construct an analytical representation for *ab initio* data in the form,

$$U(R,\hat{\omega}) = 4\pi \left\{ \exp[A(\hat{\omega}) - B(\hat{\omega})R] - \sum_{n=6,8} F_n(R,\hat{\omega}) \frac{C_n(\hat{\omega})}{R^n} + \sum_{p=5,7,9} \frac{D_p(\hat{\omega})}{R^p} \right\} \quad (1)$$

where R is the intermolecular separation, $\hat{\omega}$ denotes the three angles θ_a, θ_b, and φ describing the relative orientation of the molecules, and $F_n(R,\hat{\omega})$ is a damping function. Hereafter, we use the notation $(\theta_a, \theta_b, \varphi)$ to specify the relative orientation of the two molecules. In Eq. (1), the exponential term corresponds to the overlap repulsive contribution to the interaction energy. The two-term summation is the damped dispersion part of the interaction, and the three-term summation represents the electrostatic

interaction between quadrupole and hexadecapole moments of two molecules. The functions A, B, C_n, and D_p are intermediate parameters responsible for the angular dependence of interaction and are related to the final parameters via a spherical expansion [1].

It must be mentioned that, in some orientations, this potential exhibits a small long-range maximum. This maximum seems to be an artifact of the quadrupole–quadrupole term. This unphysical feature of the surface is very small, and its effect on the calculated properties is insignificant.

2.2. Second Virial Coefficients

One of the quantities relevant to evaluating the overall strength of the interaction over its range of action is the second virial coefficient, $B(T)$, where T is the absolute temperature. This quantity for gases gives information about the average "size" of the potential and is sensitive to the volume of the well at low temperatures, and to the hard core of the potential at high temperatures ($k_B T$ much greater than the well-depth, where k_B is Boltzmann's constant). Despite the fact that good agreement with $B(T)$ might reflect some cancellation of errors, this quantity is seen to provide a useful test of the PES, and can be used to discriminate between the surfaces.

The classical contribution to the second virial coefficient for two linear molecules takes the form [6],

$$B^{(0)}(T) = \frac{N_A}{4} \int_0^\infty R^2 dR \int d\hat{\omega}(1 - \mathrm{e}^{-\beta U}) \tag{2}$$

where N_A is Avogadro's constant, U is the intermolecular potential energy, and $\beta \equiv 1/k_B T$. Hereafter, integration over $\hat{\omega}$ denotes the triple integral over relative orientations of two molecules as

$$\int d\hat{\omega} \equiv \int_{-1}^{1} d(\cos\theta_a) \int_{-1}^{1} d(\cos\theta_b) \int_0^{2\pi} d\phi \tag{3}$$

According to the formalism developed by Pack [2], the first-order quantum correction of $B(T)$, which contains the translational $B_{tr}^{(1)}(T)$, rotational $B_{rot}^{(1)}(T)$, and coriolis $B_{cori}^{(1)}(T)$ contributions can be written as

$$\begin{aligned} B^{(1)}(T) &= B_{tr}^{(1)}(T) + B_{rot}^{(1)}(T) + B_{cori}^{(1)}(T) \\ &= -\frac{N_A \beta^2}{48} \int_0^\infty R^2 dR \int d\hat{\omega} \mathrm{e}^{-\beta U} (\hat{H}^{(0)} U) \end{aligned} \tag{4}$$

where $\hat{H}^{(0)}$ is the translation–rotation Hamiltonian operator.

Another quantity which is relevant for testing the PES is the second acoustic virial coefficient β_a. It is related to the ordinary second virial coefficient $B(T)$ and its derivatives by the following equation:

$$\frac{1}{2}\beta_a = B + P_a T\left(\frac{dB}{dT}\right) + Q_a T^2\left(\frac{d^2B}{dT^2}\right) \tag{5}$$

in which P_a and Q_a are functions of the perfect-gas heat-capacity ratio [6]. After calculating $B(T)$ at several temperatures, a smooth function has been fitted to them, and derivatives have been obtained for implementation in Eq. (5).

2.3. MMA Procedure

Mason and Monchick [3] developed their entirely classical treatment by making three basic assumptions about the dynamics of binary collisions:

(a) The effect of inelastic collisions on the trajectories is negligible.

(b) In a given collision only one relative orientation is effective.

(c) Every possible orientation has equal weight.

The physical basis for the first assumption is that the rotational energy transfer in a binary collision, for most molecules at ordinary temperatures, is much less than the translational kinetic energy and so we can neglect its effect. This assumption is expected to work best in the high-temperature limit and is inadequate for properties such as thermal conductivity that depend specifically on the transfer of internal energy. The second assumption is based on the fact that, although the potential acts along the whole trajectory, the interaction at distances around the point of closest approach mainly determines the angle of deflection, and over this small range, the relative orientation of two colliding molecules does not change much. This approximation, which is equivalent to the centrifugal-sudden approximation [4] of quantum scattering, should become better as the potential becomes more short-ranged. In summary, the MMA greatly simplifies the calculation of transport properties by replacing an angle dependent force with many central forces corresponding to different fixed orientations.

According to this approximation, the coefficients of viscosity η and self-diffusion D can be written as

$$\eta = \frac{5}{16}\left(\frac{mk_BT}{\pi}\right)^{1/2}\frac{f_\eta}{R_m^2\left\langle\Omega^{(2,2)*}\right\rangle} \tag{6}$$

$$D = \frac{3}{8n}\left(\frac{k_B T}{m\pi}\right)^{1/2} \frac{f_D}{R_m^2 \left\langle \Omega^{(1,1)*} \right\rangle} \tag{7}$$

where R_m is a distance parameter of the potential, $\left\langle \Omega^{(l,s)*} \right\rangle$ is a reduced collision integral averaged over all relative orientations, and f_η and f_D are correction factors resulting from higher-order kinetic-theory approximations [6].

Mason and Monchick assumed that all relative orientations are equally probable. With this additional assumption, the angle-averaged collision integrals are given by

$$\left\langle \Omega^{(l,s)*} \right\rangle = \frac{1}{8\pi} \int \mathrm{d}\hat{\omega} \Omega^{(l,s)*} \tag{8}$$

This equal weight approach arises naturally from the quantal IOS approximation [4]. Nowadays, there are many *ab initio* potentials which, at least for small systems, have a reasonable level of accuracy and reliability. It provides opportunities for re-examination of the MMA procedure.

Validity of the MMA results has also been tested previously by Heck et al. [7, 8] via a comparison with full classical trajectory (CT) calculations. For nitrogen the MMA viscosity cross sections differed from those obtained from the CT approach by, at most, 5% [7], and for carbon monoxide, differences of up to 10% have been observed [8]. Furthermore, in the case of carbon dioxide, Vesovic et al. [9] have obtained smaller deviations (at most 3.4%). However, they have traced this rather surprising agreement to the cancellation of MMA errors in estimating two terms that enter the viscosity cross section. In all cases deviations between MMA and CT values decrease with increasing temperature.

Such comparisons show that in all investigations the MMA approach overestimates the CT values of viscosity collision integrals (except at very low temperatures) [7–9]. Thus, with an exact potential energy the MMA viscosity coefficients will be smaller than accurate experimental results. This conclusion about the relative sign of errors introduced by MMA is important for interpreting the results of this study, since we are interested on the errors introduced by the potential energy.

3. RESULTS AND DISCUSSION

3.1. Second Virial Coefficients

Many measured second virial coefficients $B(T)$ for N_2 are available and cover a temperature range of 75–700 K [10]. Some recent data for second virial coefficients from $p\rho T$ measurements are also given by

Table I. Calculated Classical and Quantum Contributions to Second Virial Coefficient in Comparison with Experimental Results. (All values are in units of $10^{-6}\,m^3 \cdot mol^{-1}$)

T/K	$B^{(0)}$	$B_{tr}^{(1)}$	$B_{rot}^{(1)}$	$B_{cori}^{(1)}$	B_{tot}	Nowak et al. [11]
98	−166.98	0.90	0.70	0.035	−165.338	−166.5 ± 0.8
110	−134.46	0.67	0.50	0.025	−133.260	−133.8 ± 0.5
120	−113.93	0.54	0.40	0.020	−112.974	−113.12 ± 0.4
140	−84.06	0.37	0.27	0.013	−83.405	−83.06 ± 0.25
170	−55.35	0.25	0.17	0.008	−54.930	−54.23 ± 0.25
220	−27.92	0.15	0.09	0.005	−27.673	−26.81 ± 0.25
240	−20.69	0.13	0.08	0.004	−20.483	−19.61 ± 0.25
280	−9.82	0.10	0.06	0.003	−9.665	−8.77 ± 0.25
320	−2.07	0.08	0.05	0.002	−1.950	−1.09 ± 0.25
340	1.01	0.07	0.04	0.002	1.122	1.97 ± 0.25

Nowak et al. [11]. Table I presents the calculated classical and quantum contributions to the second virial coefficient and compares our calculated $B(T)$ with experimental data. Corresponding deviations $(B_{\text{cal}} - B_{\text{exp}})$ are shown in Fig. 1. It can be seen from Table I that the quantum corrections are only significant at lower temperatures, where their magnitudes are greater than the experimental uncertainty. At 75 K their sum constitutes about 1.3% of the magnitude of the classical component. By 700 K, this is reduced to about 0.15%. The coriolis term is always small. The predicted Boyle temperature of our potential, 332.4 K agrees with the experimental value of 326.8 K [14] (obtained from a smooth fit of values reported by Nowak et al. [11]) within 2%.

Our potential fails to represent the experimental data within the error bars except at low temperatures. It yields a virial coefficient that is lower than experimental data at all temperatures above 125 K. At all temperatures greater than 100 K, the deviations are within $1\,cm^3 \cdot mol^{-1}$. At lower temperatures, the calculated $B(T)$ lies higher than experiment. Relative to the more accurate results of Nowak et al. [11], the largest deviation occurs at 98 K and has a magnitude of $1.16\,cm^3 \cdot mol^{-1}$. However, noting that our new potential emerges directly from the full *ab initio* calculations, without any experimental adjustment, the overall agreement is reasonable.

Furthermore, Ewing and Trusler [12] and Estela-Uribe and Trusler [13] measured the acoustic second virial coefficientβ_a. Deviations between calculated and experimental values of acoustic second virial coefficient $(\beta_{\text{a,cal}} - \beta_{\text{a,exp}})$ have been plotted in Fig. 2. As can be seen, deviations of the acoustic virial coefficient have the same pattern as the volumetric values.

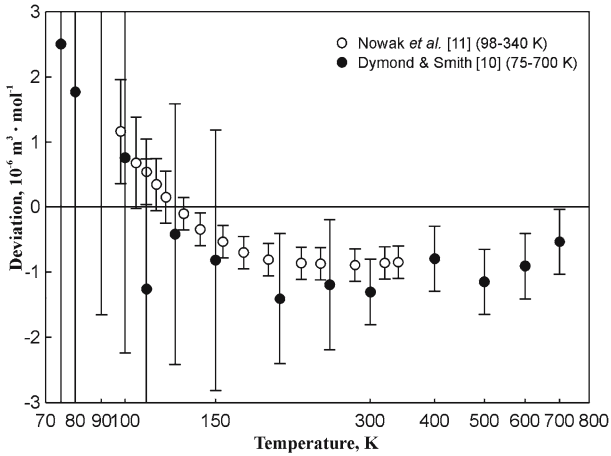

Fig. 1. Deviations between our calculated second virial coefficients and those obtained via different experiments [10, 11]. Note that the scale of temperature is logarithmic.

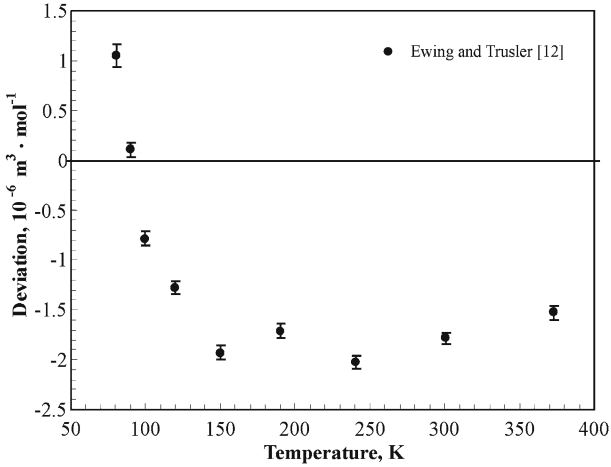

Fig. 2. Deviations between calculated and experimental second acoustic virial coefficients [12].

3.2. Numerical Analysis of MMA

In Fig. 3 the reduced potential energy is plotted as a function of reduced intermolecular separation for some fixed orientations with $\theta_a = \varphi = 0$. Their corresponding reduced cross sections $Q^{(2)*}$ are shown in

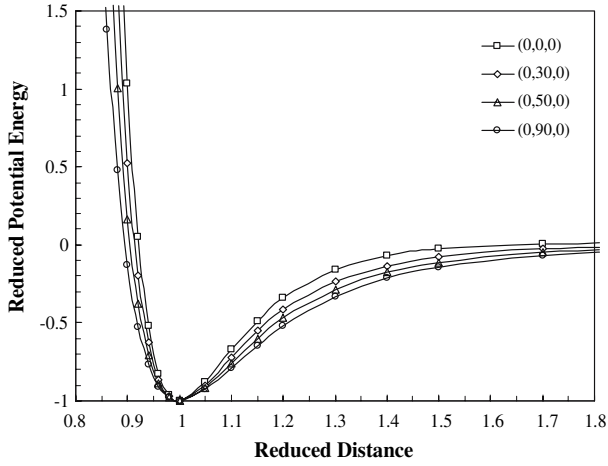

Fig. 3. Radial dependence of reduced potential energy for some fixed orientations.

Fig. 4 as a function of reduced energy of collision on a logarithmic scale. As can be seen, the cross sections of different orientations diverge at low and high energies, but there is an intersection point at intermediate energies. The curves of $\ln Q^{(2)*}$show a nearly linear behavior for both high and low energies. Similar behavior has been observed in the energy dependence of $Q^{(1)*}$ that is not represented here. Noting that the most attractive potential at long range is the least repulsive one at short range (Fig. 3), the inversion of the ordering of the $\ln Q^{(2)*}$ curves at the intersection point in Fig. 4 can be interpreted as follows.

With increasing energy of collision, the cross sections are determined by the influence of repulsive forces through head-on collisions. Thus, the curves in the high energy range of Fig. 4 are ordered according to the strength of the short-range repulsive part of the potential. At low energies, the cross sections are determined dominantly by the grazing collisions. Due to the attractive forces, there is only a gradual deflection of one molecule with respect to the other for a wide range of impact parameter values. Thus, in the low-energy part of Fig. 4 the curves are ordered according to the strength of the long- range attractive part of the potential.

We can now conclude that the high and low energy differences between cross sections correspond to the short- and long-range differences between potential curves, respectively. This correspondence can be used to determine which part of the potential is sampled effectively by cross sections of different energies.

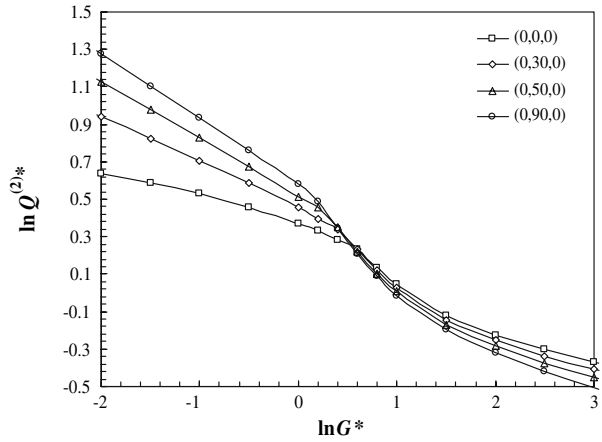

Fig. 4. Comparison of energy dependence of reduced cross sections for different orientations.

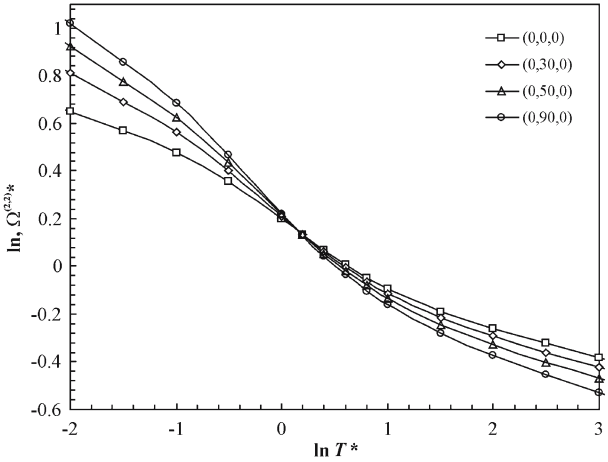

Fig. 5. Comparison of temperature dependence of reduced collision integrals for different orientations.

Behavior of the temperature dependence of $\Omega^{(2,2)}$*shown in Fig. 5 can be explained in the same way, since the averaging process of Eq. (8) emphasizes the low-energy collisions at low temperatures and the high-energy collisions at high temperatures.

The intersection point observed in Figs. 4 and 5 can be viewed as a common regularity in the MMA description of transport properties. This is also an illustrative example that provides some information about the

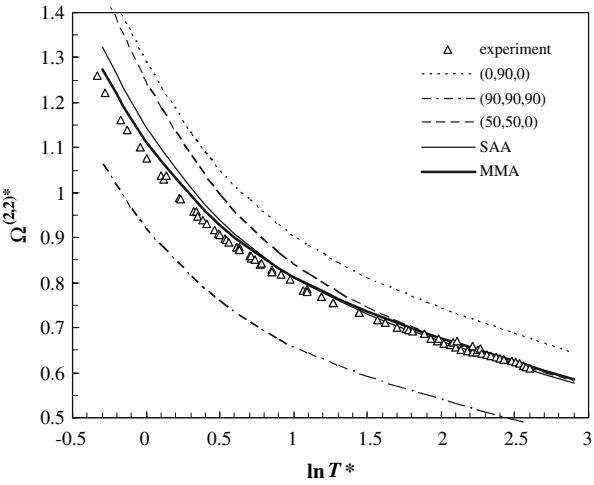

Fig. 6. Orientation-dependent collision integrals and MMA averaged values in comparison with experimental data [14–22]. SAA denotes the small anisotropy approximation [5] corresponding to (θ_0, θ_0, 90) orientation with $\theta_0 = 54.735610$.

microscopic origins of macroscopic regularities. From Figs. 3 to 5 a line is traced successively from full microscopic features of the system to a macroscopic description of it.

Figure 6 shows some orientation-dependent collision integrals and the MMA averaged integrals compared with corresponding available experimental data from $T^* = 0.72$ to $T^* = 13.51$. It contains a small portion of our calculations that are represented in Fig. 5, and according to the above conclusions about crossover points, it suggests that the temperature range covered by experimental data is mostly sensitive to the short and intermediate ranges of potentials of different orientations. It must be noted that in Figs. 3–5 the quantities of each orientation are reduced by ε and R_m of its own potential but in Fig. 6 all collision integrals of different orientations are reduced by ε and R_m of the global minimum orientation. This reduction procedure is required for consistent averaging in Eq. (8), and as a result of it, there is not a common intersection point in Fig. 6. Values of $\Omega^{(2,2)*}_{\text{exp}}$ are obtained from the experimental viscosity [14–22].

At most temperatures covered by experimental data, the upper and lower limits of angle-dependent collision integrals belong to the linear (0,0,0) (not plotted in Fig. 6), and crossed (90,90,90) orientations, respectively. In Fig. 6 the curve corresponding to the global minimum orientation (50,50,0) lies higher than the MMA, and experimental curves,

except at higher temperatures. However, at the short range of the potential the (50,50,0) orientation is not the most stable. We also represent in this figure the values corresponding to the $(\theta_0, \theta_0, 90)$ orientation (with $\theta_0 = 54.735610$) which can be used as a small anisotropy approximation (SAA) [5]. Noting the simplicity of this approximation, its agreement with MMA and experiment is relatively good except at lower temperatures.

As can be seen, it is difficult to extract decisive information about the probability of different orientations, and we can only say that, deviations between the collision integrals and experiment are strongly temperature dependent and so any weighting scheme that one might design to apply to Eq. (8) must have a temperature-dependent weight factor.

3.3. Viscosity and Diffusion Coefficients

Calculated viscosity coefficients from the MMA approach have been compared with different experimental results [14–22], most of which contain absolute measurements of η, and their reported uncertainty ranges from 0.15% to 1% [14–20]. We have also used the values reported by Dawe and Smith [21] and Guevara et al. [22] which contain measurements relative to reference values at 293.2 and 283.2 K, respectively. These data have been placed on an absolute scale using more recent and accurate measurements [17] as reference values. Deviations are defined as $(\eta_{\text{cal}} - \eta_{\text{exp}})\,100/\eta_{\text{exp}}$ and plotted against $\ln T$ in Fig. 7. The agreement between calculation and experiment becomes better with increasing temperature and is within 1% for $500\,\text{K} < T < 2150\,\text{K}$. According to the conclusions drawn at the end of Section 2.3, it can be predicted that the points in Fig. 7 will shift to more positive values if the calculations are repeated with the more accurate CT approach. However, this shifting may or may not lower the magnitude of deviations. In Fig. 7, a comparison has been also made between the small anisotropy approximation (SAA) and other data. Its agreement with experiment is reasonable at temperatures above 500 K.

Figure 8 shows the percent deviations of different calculated relative diffusion coefficients $D(298\,K)/D(T)$ from experimental values of Vugts et al. [23], whose reported uncertainty is 0.1%. The agreement of MMA values with experiment is within 1% at most temperatures, and again the SAA provide a good estimate of the more expensive MMA results.

In summary, we can say that there is reasonable agreement between the calculated transport properties obtained from our potential and those of experiment. However, from a transport-properties point of view, a classical trajectory (CT) calculation would provide a final judgment about the performance of this potential.

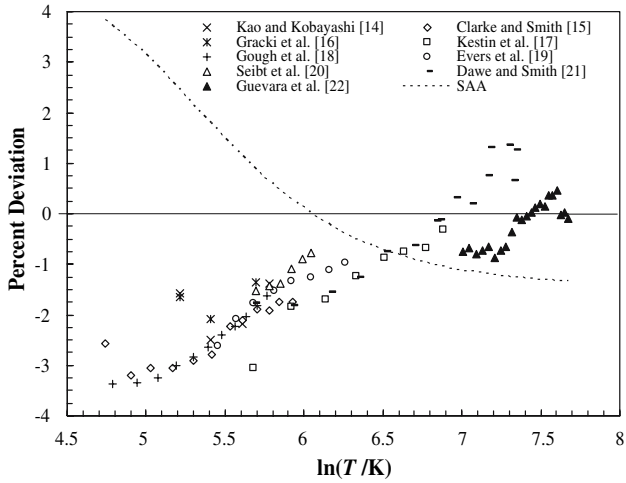

Fig. 7. Percent deviations between experimental [14–22] and MMA calculated viscosities obtained from second-order kinetic-theory approximations. SAA curve represents percent deviation between SAA and MAA results.

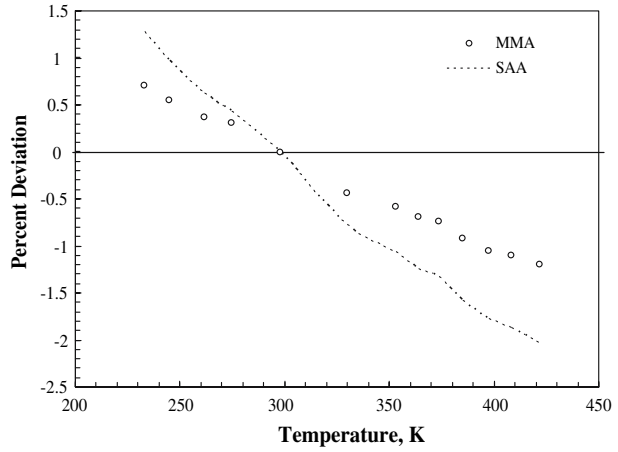

Fig. 8. Percent deviations between experimental [23] and calculated relative diffusion coefficients obtained from first-order kinetic-theory approximations.

4. CONCLUSION

In this work, we have tested a new *ab initio* N_2–N_2 potential energy surface that we have recently proposed [1]. The formalism developed by Pack [2] has been used for calculation of the second virial coefficient. In the present study quantum corrections for the second virial coefficient were significant only at lower temperatures. Noting that the potential has been calculated at the MP2/QZ level of *ab initio* theory, the overall agreement between calculated and experimental second virial data is reasonable and confirms our previous predictions [1]. However, deviations that for most temperatures are within $1\,cm^3 \cdot mol^{-1}$, suggest that a slight re-scaling of the *ab initio* potential would be beneficial.

The viscosity and diffusion coefficients have been calculated using the Mason–Monchick approximation. In a numerical analysis of this approach, we have found that the reduced cross sections and collision integrals for different fixed orientations show a common intersection point in energy and temperature diagrams, respectively. We have interpreted this regular behavior with the aim of reduced potential energy curves for different fixed orientations. As mentioned in this work, the observed intersection point can be used to determine in each specified energy range to what part of the potential the cross sections are sensitive.

In the case of transport properties, calculated and experimental results show an average deviation of about 1.6% and 0.7% for viscosity and relative diffusion coefficients, respectively. Inclusion of second-order kinetic-theory corrections improves the agreement by about 0.5% for the case of absolute results. The overall agreement between the experimental data and those obtained from the *ab initio* surface is reasonable under the MMA assumptions.

ACKNOWLEDGMENT

We are thankful to the Research Council of the University of Tehran for their support of this work.

REFERENCES

1. M. H. Karimi Jafari, A. Maghari, and S. Shahbazian, *Chem. Phys.* **314**:249 (2005).
2. R. T. Pack, *J. Chem. Phys.* **78**:7217 (1983).
3. L. Monchick and E. A. Mason, *J. Chem. Phys.* **35**:1676 (1961).
4. G. A. Parker and R. T. Pack, *J. Chem. Phys.* **68:**1585 (1978).
5. J. R. Stallcop, H. Partridge, and E. Levine, *Phys. Rev*. **A 62**:062709 (2000).
6. J. O. Hirschfelder, C. F. Curtiss and R. B. Bird, *Molecular Theory of Gases and Liquids* (John Wiley & Sons, Inc., New York, 1964).

7. E. L. Heck, A. S. Dickinson, and V. Vesovic, *Chem. Phys. Lett.* **204:**389 (1993).
8. E. L. Heck, A. S. Dickinson, and V. Vesovic, *Chem. Phys. Lett.* **240:**151 (1995).
9. V. Vesovic, S. Bock, E. Bich, E. Vogel, and A. S. Dickinson, *Chem. Phys. Lett.* **377:**106 (2003).
10. J. H. Dymond and E. B. Smith, *The Second Virial Coefficients of Pure Gases and Mixtures* (Oxford University Press, Oxford, 1980).
11. P. Nowak, R. Kleinrahm, and W. Wagner, *J. Chem. Thermodyn.* **29**:1137 (1997).
12. M. B. Ewing and J. P. M. Trusler, *Physica A* **184**:415 (1992).
13. J. F. Estela-Uribe and J. P. M. Trusler, *Int. J. Thermophys.* **21**:1033 (2000).
14. J. T. F. Kao and R. Kobayashi, *J. Chem. Phys.* **47:**2836 (1967).
15. A. G. Clarke and E. B. Smith, *J. Chem. Phys.* **48:**3988 (1968).
16. J. A. Gracki, G. P. Flynn, and J. Ross, *J. Chem. Phys.* **51:**3856 (1969).
17. J. Kestin, S. T. Ro, and W. A. Wakeham, *J. Chem. Phys.* **56:**4036 (1972).
18. D. W. Gough, G. P. Matthews, and E. B. Smith, *J. Chem. Soc. Faraday Trans. I* **72**:645 (1976).
19. C. Evers, H. W. Lösch, and W. Wagner, *Int. J. Thermophys.* **23**:1411 (2002).
20. D. Seibt, E. Vogel, E. Bich, D. Buttig, and E. Hassel, *J. Chem. Eng. Data* **51**:526 (2006).
21. R. A. Dawe and E. B. Smith, *J. Chem. Phys.* **52:**693 (1970).
22. F. A. Guevara, B. B. McInteer, and W. E. Wageman, *Phys. Fluids* **12**:2493 (1969).
23. H. F. Vugts, A. J. H. Boerboom, and J. Los, *Physica* **50**:593 (1970).